論文 / 著書情報
Article / Book Information

論題(和文)	
Title(English)	Characteristics of an Atmospheric Pulsed DBD Plasma Jet and Its Preliminary Application for Strilization
著者(和文)	ﾘ ｺｳ, 坂井 奈津子, 渡邊 正人, 堀田 栄喜, 和地 正明
Authors(English)	J.Li, N.Sakai, M.Watanabe, E.Hotta, M.Wachi
出典(和文)	Physics and Application of Plasmas Based on Pulsed Power Technology,　NIFS-PROC-90, pp. 82-87
Citation(English)	Physics and Application of Plasmas Based on Pulsed Power Technology,　NIFS-PROC-90, pp. 82-87
発行日 / Pub. date	2012,　4

Characteristics of an atmospheric pulsed DBD plasma jet and its preliminary application for sterilization

Jia Li[a], Natsuko Sakai[a], Masato Watanabe[a], Eiki Hotta[a] and Masaaki Wachi[b]

[a] *Department of Energy Sciences, Tokyo Institute of Technology, 4259 Nagatsuta, Midori-ku, Yokohama, 226-8502 Japan*

[b] *Department of Bioengineering, Tokyo Institute of Technology, 4259 Nagatsuta, Midori-ku, Yokohama, 226-8502 Japan*

A novel plasma jet with a plane-to-plane DBD structure working at atmospheric pressure is developed. This jet is operated at a sub-microsecond pulsed voltage with a repetition rate of 1-10 kHz range. The working gas, helium, is fed into the plasma jet. The electrical property of the discharge has been studied by means of a classical DBD model. By fitting the fine structure of the emission bands of N_2, plasma gas is found to be cooled to be near room temperature (~ 300 K) at the position of 15 mm away from the jet nozzle exit, which is also verified by a thermocouple. Based on the analysis of the H_β Stark broadening, the electron density inside the plasma jet nozzle is evaluated to be in the order of 10^{14} cm^{-3}. Finally, the feasibility of disinfecting E.coli cells was confirmed preliminarily.

Keyword: dielectric barrier discharge, plasma jet generation, gas temperature, electron density, sterilization

I. INTRODUCTION

Recently, non-thermal atmospheric pressure plasma jets operated at atmospheric pressure have been attracting significant attention due to some marked merits, such as without expensive vacuum units and promising potentials in a variety of applications like thermally sensitive materials treatment [1-3]. Especially, the biomedical applications using such plasma jets have become hot issues. To extend the plasma treatment to living tissue, one of the prerequisites is that the jet should be near the room temperature and carries a low current under moderate voltage. Moreover, at the point of applications, it is necessary to attain high plasma stability while maintaining efficient reaction chemistry.

The atmospheric pressure plasma jet can be realized in various configurations utilizing different types of excitation from DC to microwave frequency. Usually, their generation relies on several mechanisms: capacitively coupled discharge (CCP), corona discharge, and dielectric barrier discharge (DBD) [4-7]. Among them, the major advantage of DBD configuration is to effectively prevent spark-to-arc transition and hence to stabilize the discharge. Concerning power excitation, recent results by Laroussi M and Lu X [8] have shown that sub-microsecond pulsed voltages at kilohertz frequency can provide a great capability to control the plasma jet ignition and to reduce the gas temperature.

In this paper, a novel plasma jet with a plane-to-plane DBD structure driven by sub-microsecond pulsed power at atmospheric pressure is developed, whereby stable non-thermal plasma in helium can be generated. The main aim of this study is to understand the plasma characteristics by measuring and analyzing basic plasma parameters such as gas temperature and electron density. Finally, the possibility of bacterial inactivation was investigated preliminarily.

II. EXPERIMENTAL SETUP

Figure 1 shows the schematic illustration of the experimental setup. As shown in Fig.1 (a), it mainly consists of three parts: the plastic case, the main unit where discharges occur and the high voltage (HV) generator. The plastic case works as a pathway for plasma gas as well as fixing the main unit. The main unit, whose detailed structure is shown in Fig.1 (b), has a plane-to-plane DBD structure. Two parallel glass plates (50×7×1 mm, $\varepsilon_r = 10$) are inserted into the square opening (7×3 mm) on the plastic case and stabilized by adhesive. They serve as dielectric barrier layers with 1 mm gap spacing. Electrodes are two right-angled copper plates with the longer parts (15×7×1 mm) attached to the surface of these glass plates tightly. The shorter parts are fastened to the plastic case by screws. To prevent the gas leaking from the sides, two parallel glass plates are stuck to the side faces. All the parts of the device are fixed to each other to prevent accidental displacement. The working gas of Helium (99.9%) with a flow rate (f) up to 20 liters per minute (l/min) is injected through the rear hole of plastic case controlled by a mass flow controller and flow out of the nozzle exit.

A homemade sub-microsecond HV pulse generator [9] was used in this work. This unipolar generator employs an inductive energy storage system with an SI Thyristor as a current interrupter. The typical characteristics are: voltage amplitude ~ 20 kV, pulse width ≤ 500 ns and pulse repetition rate (PRR) ~ 10 kHz. A current limiting resistor 2 kΩ is connected in series between the HV pulse generator and plasma jet device.

Once the helium gas is introduced and high voltage is applied, a discharge is fired in the gap between the parallel glass plates. The plasma gas of the discharge is spewed out from the jet nozzle and a plasma plume reaching length of about 3 cm at 4 l/min is ejected to open air, as shown Fig.1 (c). Here, the plasma jet images were recorded by Nikon digital camera D40X with an exposure time of 10 s. Also, the Reynolds number (Re) in such helium plasma jet device can be estimated from $Re = D \cdot v \cdot \rho / \mu$, where v is helium velocity, ρ is helium density (0.164 kg/m^3), and μ is helium viscosity (2×10^{-5} kg/m s) at 20 °C and at 1 atm., D is the characteristic length or hole diameter. For rectangular ducts, as in the case of our experimental setup, D is defined as 4 times the cross-sectional area, divided by the wetted perimeter [10] and is calculated to be 1.75 mm. Then Re is calculated to be 136.66, showing the production of helium plasma jet in laminar flow [11].

An optical fiber is positioned radially at 1 cm away from the side face of main unit and can be freely moved along the axis. The optical emission collected by the optical fiber is recorded by two spectrometers: Ocean Optics Maya 2000 for wavelength in the range of 200-800 nm, and a UV-visible MD-25 spectrometer (Japan Spectroscopic Co.) with

a linear CCD multi-channel detector. The latter has a grating of 1800 g/mm and slit width of 100 μm and is used to measure the spectrum of N_2 $C^3\Pi_u \rightarrow B^3\Pi_g$ (372-382.5 nm), N_2^+ $B^2\Sigma_u^+ \rightarrow X^2\Sigma_g^+$ (387-392 nm) and H_β line.

III. RESULTS AND DISCUSSION

A. Electrical characteristic of the plasma

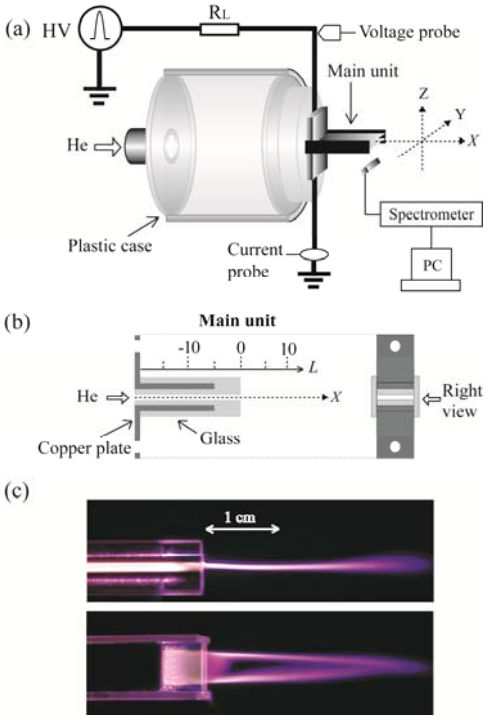

Figure 1. Schematic of the experimental setup. (a) DBD plasma jet (*X*, *Y* and *Z* are axes of rectangular coordinates.). (b) Detailed structure of main unit (L: axial position in mm). (c) Photographs of the He plasma plume in both *Y* and *Z* viewing directions under the conditions of V_d = 13 kV, PRR = 5 kHz and f = 4 l/min.

Employing a rather classical model, the equivalent circuit of our set-up is given in Fig.2. The DBD reactor, i.e. the main unit, is modeled by a capacitor C_d representing the solid dielectric connected in series with the gas gap. The latter is the parallel combination of a C_g capacitor and a R_p resistor, corresponding to the pure gas capacitance and the plasma resistance, respectively. Parallel to the DBD reactor, there is a C_c representing all the parasitic capacitances that can be deduced from measurements when plasma is off. A fictitious switch S is drawn on the circuit to denote that plasma occurs intermittently. The measured applied voltage and overall current flowing in the circuit are noted as V_d *(t)* and i_{total} *(t)*, respectively. It is noted that i_{total} *(t)* includes both a displacement i_{dis} *(t)* and conduction components i_z *(t)*. Applying circuit theory to this equivalent circuit, basic electrical properties of the DBD plasma can be deduced, as shown in the following equations (S switch being on) [19]:

$$i_z(t) = \left(1 + \frac{C_g}{C_d}\right) i_{total}(t) - C_g \frac{dV_d(t)}{dt} \qquad (1)$$

$$V_g(t) = V_d(t) - V_m(t) = V_d(t) - \frac{1}{C_d}\int_{t_0}^{t} i_{total}(\tau)d\tau \qquad (2)$$

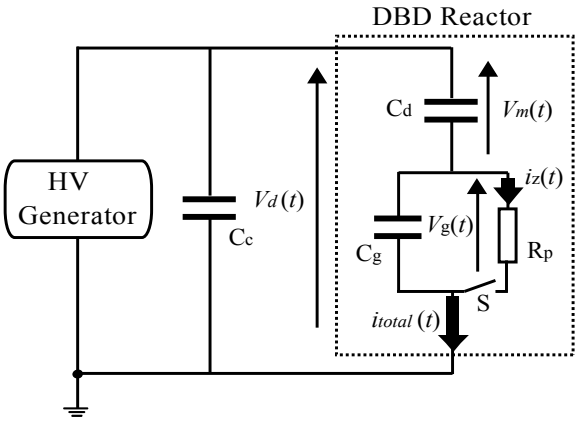

Figure 2. Equivalent electrical circuit.

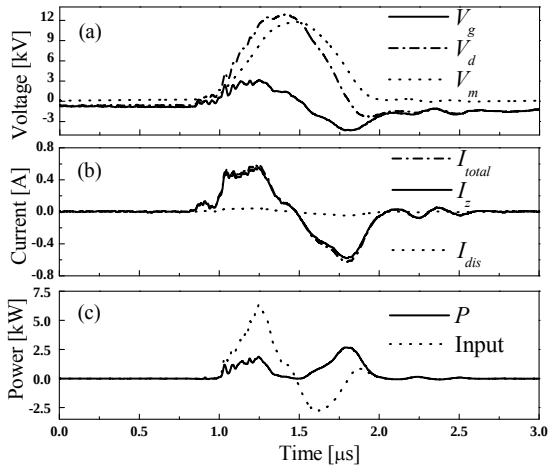

Figure 3. Voltage, current and power waveforms for the He plasma jet under the conditions of V_d = 13 kV, PRR = 10 kHz and f = 2 l/min.

$$P(t) = V_g(t) \cdot i_z(t) \qquad (3)$$

where *P (t)* is plasma power. For the electrical study, a program was made to solve numerically the above equations, where the experimentally obtained V_d *(t)* and i_{total} *(t)* waveform data are fed as input variables. For numerical stability reasons the experimental signals are fitted by means of cubic interpolating polynomials. Results are shown in Fig.3. It can be seen that though the applied voltage is unipolar pulse, the current appears bipolar and has both positive and negative pulses, indicating that two discharges started in the rising and falling phase of the applied pulse, respectively. Fig.3 (b) shows that initially the gap voltage V_g increases following the applied voltage V_d. Then, as the discharge onset voltage is attained, the positive conduction current pulse occurs. This charges the dielectric, i.e., V_m increases, as shown in Fig.3 (a), and induces a significant drop in V_g resulting in the positive discharge extinction. Next, during the falling flank of V_d, the already charged dielectric induces a significant negative gap voltage which is sufficient to ignite a negative discharge. It is noteworthy that, as shown in Fig.3 (c), during the negative discharge, some power stored during the primary discharge in the circuit's capacitive elements is actually returned to the HV generator [12-13].

B. Plasma emission

To investigate what kinds of excited species presented in the plasma, the aforementioned spectrometer (Maya 2000) is used to measure the optical emission of plasma plume. All spectral plots are the result of 5 data acquisitions. Spectral species identification, labeling and relative intensity measurements were done by using the Spectrum Analyzer (version 1.7) software [14].

A typical emission spectrum of the helium plasma in the range of 200-800 nm obtained at the nozzle exit (L = 0 mm) is shown in Fig. 4. It shows that there are strong nitrogen molecular lines as well as a few helium and oxygen atomic lines. The strongest emission is the excited He atom line at 706.5 nm, and N_2 ($C^3\Pi_u \rightarrow B^3\Pi_g$) band at 337.1 nm and excited oxygen line ($3p\ ^5P \rightarrow 3s\ ^5S$) at 777.3 nm are shown.

Oxygen and nitrogen species arise because the plasma is ejected into the ambient air where its energetic electrons and He metastables ionize and excite air molecules. The N_2^+ line at 391.4 nm is attributed to Penning ionization and charge transfer [15] followed by direct electron-impact excitation. Atomic oxygen is generally generated by a dissociative collision between an oxygen molecule and an electron. Atomic oxygen may also be generated though Penning ionization [16]. Moreover, the emission band of the OH radical at 308.9 nm is shown in the spectrum. The OH radicals represent the result of the dissociation of H_2O molecules from the humid back-diffused air caused by collisions with accelerated electrons or with long-lived species present in the plasma, especially helium metastables[17].

To observe qualitatively the behavior of the plasma species along the axial direction, we selected four representative lines: He – 706.5 nm as plasma gas, N_2 – 337.1 nm as the dominant component of the diffusing air, O – 777.4 nm as species crucial for biomedical treatment and N_2^+ – 391.4 nm as an indicator of helium metastable presence.

Figure 5 portrays the peak intensity of selected emission line as a function of axial position L. For better distinction, the emission intensity of the species other than He is normalized to 1/5 of the peak intensity of He 706.5 nm line. As can be seen, the He 706.5 nm decays as soon as the plasma plume propagates out of the discharge zone between parallel electrodes (L ≥ -5 mm). The reason may be due to its high excitation energy (23.07 eV) and thus sensitive to the intensity of electric field. The emissions of the air originating species (N_2^+, O) present peaks at the same position, the nozzle exit (i.e. L = 0 mm). This is the place corresponding to the most favorable combination between the electric field strength and the back-diffusion of air into the plasma column to excite the species. Inside the jet nozzle, although the electric field is very intense, the back-diffusion of air is low, and away from the jet nozzle the back-diffusion of air is high while the electric field strength decreases. The N_2 337.1 nm line increases slowly and reaches its maximum at about 5 mm away from the nozzle exit. This may be explained as follows. The threshold energy of N_2 ($C^3\Pi_u$) state is much lower than that of N_2^+ ($B^2\Sigma_u^+$) and O ($3p\ ^5P$). Therefore, N_2 ($C^3\Pi_u$) state can still be generated through various processes such as step excitation and pooling reaction ($2N_2$ ($A^3\Sigma_u^+$) → N_2 ($C^3\Pi_u$) + N_2 ($X^1\Sigma_g^+$)) [18]. This process was found to be the dominant production mechanism of the C-state in the afterglow of He/N_2 plasmas in DBD at atmospheric pressure [19].

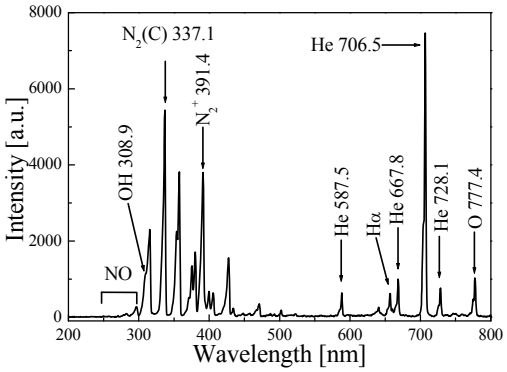

Figure 4. Emission spectra at the axial position L=0 mm under the conditions of V_d = 13 kV, PRR = 10 kHz and f = 2 l/min.

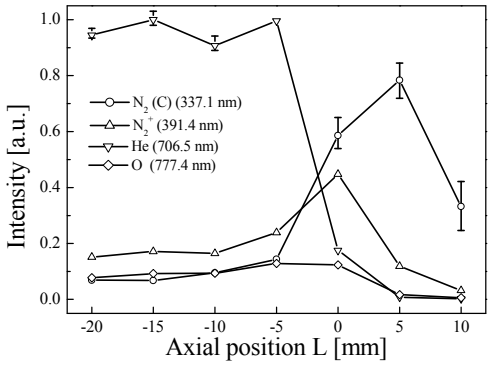

Figure 5. Dependence of selected N_2 (C), N_2^+, He and O atom normalized line intensities on the axial position L. Experimental conditions are same as that of Fig.4.

C. Excitation temperature and Gas temperature

To have a further insight into the plasma characteristics, the excitation temperature is obtained provided that the population in the levels of atom follows the Boltzmann distribution for plasma in the local thermodynamic equilibrium. Based on the optical emission spectrum shown in Fig.4, the characteristic spectral lines 587.56, 667.82, 706.5, and 728.13 of He atoms are chosen for approximation. After calculation, the T_{exc} is found to be around 1123 K.

Gas temperature T_g is another important parameter to evaluate non-thermal plasma behavior and some parameters, like electron density, are dependent on T_g. Also, it is quite important when plasmas are to be applied to biomedical processing. Generally, T_g increases with applied voltage and pulse repetition rate while decreases with flow rate.

For non-thermal plasma, T_g can be usually deduced from the rotational temperature T_r of diatomic species, such as N_2, N_2^+ and OH. The rotational temperature describes the population of the rotational levels in molecular species. The distribution, unlike that of vibrational levels, is not given by a pure Boltzmann distribution. Each rotational level has a different statistical weight due to the (2J+1)-fold degeneracy of the states, where J is the total angular momentum of the molecule. Therefore, the thermal distribution of the rotational states will be given by the product of the Boltzmann factor exp(-E/kT) times the statistical weight (2J+1) [20]. For most species it can be assumed that T_r is

close to the translational temperature T_t and is effectively considered to be T_g of the mixture because rotational-to-translational relaxation is fast at atmospheric pressure [15, 21, 22, 23]. Since the MD-25 spectrometer used in this paper does not resolve the rotational structure, in order to calculate the rotational temperature, we have fitted the experimental data with a theoretical calculation that takes into account the instrumental line broadening of the spectrometer.

In this work, to determine the gas temperature, the MD-25 spectrometer was used to measure the emission of N_2 $C^3\Pi_u$-$B^3\Pi_g$ (Δv = -2) band at the position L = 15 mm and then the Specair program [22, 24] was used to generate the simulated spectra and for comparison, both experimental and simulated spectra were normalized. A least-square procedure was made to obtain the best fit, which gives the rotational temperature. A typical fitting of the measured band spectrum with the simulated one is shown in Fig.6. By this way, it is found that gas temperature is already cooled to be around room temperature (300 K) at the position 15 mm away from the nozzle outlet. The gas temperature obtained from this method is in good agreement with the value (301.75 ± 0.8 K) measured by the thermocouple (CIE 305P) with a nominal error of 0.1°C. By applying the same method to simulate the emission of N_2^+ ($B^2\Sigma_u^+ \rightarrow X^2\Sigma_g^+$) band,

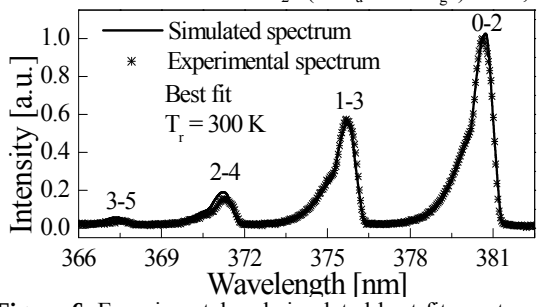

Figure 6. Experimental and simulated best-fit spectra of N_2 ($C^3\Pi_u \rightarrow B^3\Pi_g$) at L = 15 mm. Experimental conditions are: V_d = 13 kV, PRR = 10 kHz , f = 2 l/min.

the gas temperature inside the plasma jet was determined to be in the range of 360 ~ 400 K. These results will be used to calculate electron density in the next section.

D. Electron density

The spectral method for obtaining the electron density is based on the analysis of the profile broadening of the 486.13 nm H_β line. Compared to other hydrogen Balmer lines, the H_β line is often preferred because it has adequate emission intensity, higher sensitivity to electron density and lower susceptibility to self-absorption [25]. Besides the Stark broadening, the H_β line emitted from plasma (usually mixed with a little H_2) can be broadened by other mechanisms and the total broadening of the line profile is due to the combined contribution of all effects. Each broadening mechanism is independent and plays a different role on broadening the line depending on the plasma conditions. Under the experimental conditions of this work (1 atm, T_g ~ 360-400K), the only relevant sources of broadening are the Stark broadening, the van der Waals broadening, the Doppler broadening and the instrumental broadening. Other less important effects such as resonance broadening can be ignored due to the small amount of H_2 addition.

The total H_β lineshape can be approximated with a Voigt function, resulting from a convolution of Gaussian and Lorentzian profiles. The full-width at half maximum (FWHM) of both the Gaussian and Lorentzian components, $\Delta\lambda_G$ and $\Delta\lambda_L$, are given in Eq. (4) and (5), respectively

$$\Delta\lambda_G = \sqrt{\Delta\lambda_{Doppler}^2 + \Delta\lambda_{Instrument}^2} \quad (4)$$

$$\Delta\lambda_L = \Delta\lambda_{Van\,der\,Waals} + \Delta\lambda_{Stark} \quad (5)$$

where $\Delta\lambda_{Doppler}$, $\Delta\lambda_{Instrument}$, $\Delta\lambda_{Van\ der\ Waals}$ and $\Delta\lambda_{Stark}$ are the FWHM of Doppler, instrumental, Van der Waals and Stark broadening, respectively. The part of the line broadening corresponding only to the Stark broadening can be obtained from the total broadened profile.

During the experiment, a small amount of H_2 (0.02 mol%) was added into the He gas flow and the emission emitted from plasma was recorded. The instrumental broadening was calibrated with the He–Ne laser (5 mW) on steady glow 632.8 nm, using the same experimental set-up (1800 grooves/mm gratings) and was found to be a Gaussian of FWHM 0.359 nm. Doppler broadening is due to the thermal motion of excited hydrogen atoms and is determined from the gas temperature T_g by the expression of its FWHM

$$\Delta\lambda_{Doppler} = 7.16\times10^{-7}\lambda_0\left(\frac{T_g}{M}\right)^{0.5} \quad (6)$$

where λ_0 is the emission wavelength in nm and M is the atomic weight of H atoms in gmol^{-1}. Van der Waals broadening is caused by collisions of excited H atoms (the emitters) with ground state He atoms (the perturbers). According to [21], the value of $\Delta\lambda_{Van\ der\ Waals}$ was estimated by formula

$$\Delta\lambda_{Van\,der\,Waals} \approx 4.09\times10^{-13}\lambda_0^2\left(\alpha R^2\right)^{2/5}\left(\frac{T_g}{\mu}\right)^{3/10} n_{He} \quad (7)$$

where α is the average polarizability of He, given in cm^3, and is equal to $1.38\times a_0^3$ (a_0 is the Bohr radius in cm), the parameter $R^2 \approx 600 \times a_0^2$ cm^2 is determined from the ionization energy of H and the upper and lower energy levels of the H_β, μ = 0.8 is the emitter-perturber reduced mass, and n_{He} is the neutral He gas density in cm^{-3}. Stark broadening arises from the interaction between charged particles and excited H atoms, and the FWHM of Stark broadening is related to the electron density by [26]

$$\Delta\lambda_{Stark}\left(nm\right) = 2\times10^{-11}\left(n_e\right)^{2/3} \quad (8)$$

where n_e is the electron density in cm^{-3}. The electron temperature is not considered since the electron density depends scarcely on the electron temperature for the H_β line.

The recorded H_β spectral profile was normalized to its area and then fitted to a Voigt function according to the Maquardt–Levenberg method. $\Delta\lambda_G$, calculated from equation (4), was kept constant at a given gas temperature. $\Delta\lambda_L$ was obtained from the best fit between the simulated Voigt profile and the experimental spectrum. Then, the Stark contribution, $\Delta\lambda_{Stark}$, was found from equation (5). A typical fitting is shown in Fig.7, where $n_e = 1.52\times10^{14}$ cm^{-3} is obtained from $\Delta\lambda_{Stark}$ = 0.0571 nm.

By this way, the effects of peak applied voltage, pulse repetition rate, flow rate and axial position on electron density are investigated. Results are shown in Fig.8. Electron density increases almost linearly with the pulse repetition rate and applied voltage, as shown in Fig.8 (a). With the increase of pulse repetition rate or applied voltage, electrons can gain more energy and cause more ionization collisions. On the other hand, from Fig.8 (b), it can be seen

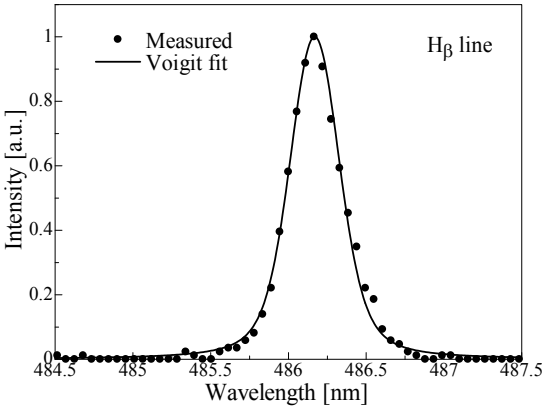

Figure 7. A typical line profile of H_β line at the position of L = -10 mm under the conditions of V_d = 8 kV, PRR = 10 kHz and f = 2 l/min. $\Delta\lambda_{Stark}$ = 0.0571 nm and electron density $n_e = 1.52\times10^{14}$ cm^{-3}.

that electron density varies inversely with the He gas flow rate. A same behavior was also found in Ar plasma jet [26]. With the increased flow rates, the gas velocity increases and the residence time of the gas in the electrode gap decreases. Consequently, the electron density becomes lower.

Figure 8 (c) reveals the electron density as a function of axial position. The pulse repetition rate was set to be 5 and 10 kHz under the conditions of 13 kV and 2 l/min. As shown in Fig.8 (c), the electron density rapidly decreases as the position is approaching the nozzle exit, due to recombination and attachment. At the position of the nozzle exit, the electron density has been 3~4 times less than that in the center of jet nozzle. Electron density away from the nozzle exit could not be determined due to the limitation of the spectrometer used here; it is reasonable to estimate that the electron density in the plasma plume should be lower, probably in the order of 10^{13} cm^{-3}. However, its confirmation needs further investigations.

E. Sterilization experiment

To confirm the feasibility of disinfecting micro-organisms, we employed the *E.coli* bacterial cells as a model micro-organism. The plasma jet was directed to the center of the Petri dish perpendicularly to its surface. The distance between surface of agar and outlet edge of plasma nozzle was 2 cm. The operational conditions were set to be f = 2 l/min, PRR = 5 kHz and V_d = 13 kV. Figure 9 presents photos of Petri dishes of 90 mm diameter, showing the distribution of bacteria population of *E. coli* on agar. It was taken after incubation over 24 h at 37 °C. Before incubation, *E. coli* was treated with plasma jet under exposure time of 4 and 8 min, respectively. By contrast with untreated culture medium growing *E.coli*, the inactivation effect is clearly seen.

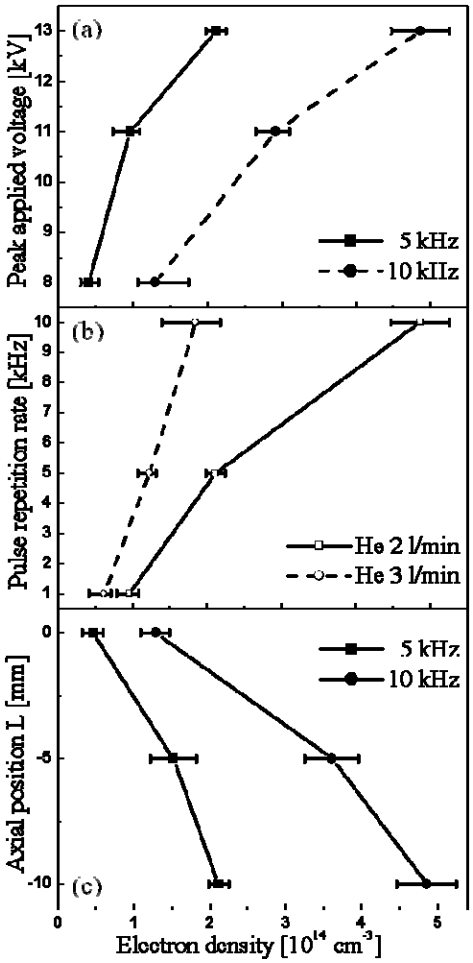

Figure 8. (a) The variation in the electron density with peak applied voltage at different pulse repetition rate. Experimental condition: f = 2 l/min; (b) The variation in the electron density with pulse repetition rate at serial of He gas flow rate of 2 and 3 l/min. Experimental condition: V_d = 13 kV; (c) The variation in the electron density with axial position at different pulse repetition rate. Experimental condition: f = 2 l/min and V_d = 13 kV.

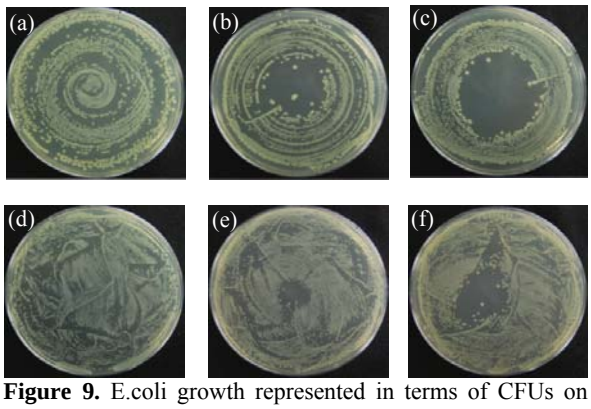

Figure 9. E.coli growth represented in terms of CFUs on agar plates, where (a) and (d) control without plasma treatment, (b) and (e) treated with 4 min and (c) and (f) treated with 8 min. CFU: (a) - (c) 5×10^3 (d)-(f) 5×10^4 .

IV. SUMMARY

A novel plasma jet with a plane-to-plane DBD structure working at atmospheric pressure is developed to create non-thermal plasma. This jet is operated at a pulsed voltage, produced by a homemade sub-microsecond pulsed power generator, with a repetition rate of 1-10 kHz range. The working gas, helium for the moment, is fed into the plasma jet. The electrical property of the discharge has been studied by means of a classical DBD model. By fitting the fine structure of the emission bands of N_2^+ and N_2, plasma gas is found to be heated inside the jet nozzle up to ~ 400 K but is cooled during transport from the nozzle exit. At the position of 15 mm away from the jet nozzle exit, the gas has been cooled to be near room temperature (~ 300 K), which is also verified by a thermocouple. The electron density is evaluated from the analysis of the Stark broadening of H_β emission and found to be in the order of 10^{14} cm^{-3} inside the plasma jet nozzle. It is shown that the electron density increases almost linearly with the applied voltage and pulse repetition rate while decays rapidly as plasma moves towards the nozzle exit. Finally, preliminary results show that this jet has potential in bacterial inactivation.

REFERENCES

[1] F. Iza, G. J. Kim, S. M. Lee, J. K. Lee, J. L. Walsh, Y. T. Zhang and M. G. Kong: "Microplasmas: Sources, particle kinetics, and biomedical applications", *Plasma Processes Polym*, Vol.5, No.4, pp.322-344 (2008)

[2] M. Laroussi and T. Akan, "Arc-Free Atmospheric Pressure Cold Plasma Jets: A Review", *Plasma Processes Polym*, Vol.4, No.9, pp.777-788 (2007)

[3] X. Zhang, M. Li, R. Zhou, K. Feng, and S. Yang: "Ablation of liver cancer cells *in vitro* by a plasma needle", *Appl. Phys. Lett.* , Vol.93, No.2, pp. 021502 (2008)

[4] T. L. Ni, F. Ding, X. D. Zhu, X. H. Wen, and H. Y. Zhou: "Cold microplasma plume produced by a compact and flexible generator at atmospheric pressure", *Appl. Phys. Lett.* , Vol.92, No.2, pp. 241503 (2008)

[5] H. S. Park, S. J. Kim, H. M. Joh, T. H. Chung, S. H. Bae and S. H. Leem: "Optical and electrical characterization of an atmospheric pressure microplasma jet with a capillary electrode", *Phys. Plasmas*, Vol.17, No.3, pp. 033502 (2010)

[6] M. Teschke, J. Kedzierski, E. G. Finantu-Dinu, D. Korzec, and J. Engemann: "High-speed photographs of a dielectric barrier atmospheric pressure plasma jet", *IEEE Trans. Plasma Sci.*, Vol.33, No.2, pp. 310-311 (2005)

[7] A. Fridman, A. Chirokov, and A. Gutsol: "Non-thermal atmospheric pressure discharges", *J. Phys. D: Appl. Phys.*, Vol.38, No.2, pp. R1-R24 (2005)

[8] Laroussi M and Lu X: "Room-temperature atmospheric pressure plasma plume for biomedical applications", *Appl. Phys. Lett.*, Vol.87, No. 11, pp.113902 (2005)

[9] J. Li, N.Sakai, M. Watanabe and E. Hotta: "A 10 kHz Sub-microsecond High-voltage Pulse Generator Using SI Thyristor for Micro-plasma Jets Generation", *IEEJ Trans.FM*, Vol.130, No.6, pp.573-578 (2010)

[10] http://en.wikipedia.org/wiki/Reynolds_number

[11] John F.O'Hanlon: A User's Guide to Vacuum Technology, 2nd ed, p. 23, New York: John Wiley (1980)

[12] E. Panousis, N. Merbahi, F. Clement, A.Ricard, M. Yousfi, L.Papageorghiou, J.F. Loiseau, O.Fichеald, B.Held and N.Spyrou: "Atmospheric Pressure Dielectric Barrier Discharges Under Unipolar and Bipolar HV Excitation in View of Chemical Reactivity in Afterglow Conditions", *IEEE Trans. Plasma Sci.*, Vol. 37, No. 6, pp. 1004–1015 (2009)

[13] Laroussi M and Lu X: "Power consideration in the pulsed dielectric barrier discharge at atmospheric pressure", *J.Appl. Phys.*, Vol.96, No. 5, pp.3028-3030 (2004)

[14] Z.Navratil, D. Trunc, R. Smid and L. Lazar: "A software for optical emission spectroscopy-problem formulation and application to plasma diagnostics",*Czech. J. Phys.*, Vol. 56, pp.B944–B951 (2006)

[15] G.Nersisyan and W. G. Graham: "Characterization of a dielectric barrier discharge operating in an open reactor with flowing helium", *Plasma Sources Sci. Technol.*, Vol. 13, No.4, pp. 582-587 (2004)

[16] R.Oikari, V. Hayrinen and R. Hernberg: "Influence of N-O chemistry on the radiative emission from a direct current nitrogen plasma jet", *J. Phys. D: Appl. Phys.*, Vol. 35, No.11, pp. *1109-1116* (2002)

[17] S. D. Anghel, A. Simon and T. Frentiu: "Spectroscopic investigations on a low power atmospheric pressure capacitively coupled helium plasma", *Plasma Sources Sci. Technol.*, Vol. 17, No.4, pp. *045016*(2008)

[18] I. Stefanovic, N.K. Bibinov, A.A. Deryugin, I.P. Vinogradov, A.P. Napartovich and K. Wiesemann: "Kinetics of ozone and nitric oxides in dielectric barrier discharges in O2/NOx and N2/O2/NOx mixtures", *Plasma Sources Sci. Technol.,Vol.10, No*. 3, pp. 406–416 (2001)

[19] N.K. Bibinov, A.A. Fateev and K. Wiesemann: "On the influence of metastable reactions on rotational temperatures in dielectric barrier discharges in He-N_2 mixtures", *J.Phys.D: Appl.Phys.*, Vol.34, No.12, pp.1819-1826 (2001))

[20] G. Herzberg: Molecular Spectra and Molecular Structure, 2nd ed, p. 124, New York: Van Nostrand(1950)

[21] Q.Wang,I. Koleva, V. M. Donnelly and D. J. Economou: "Spatially resolved diagnostics of an atmospheric pressure direct current helium microplasma", *J. Phys. D: Appl. Phys.*, Vol.38, No.11, pp. 1690-1697(2005)

[22] D.Staack, B. Farouk, A.F. Gutsol and A.A. Fridman: "Spectroscopic studies and rotational and vibrational temperature measurements of atmospheric pressure normal glow plasma discharges in air", *Plasma Sources Sci. Technol.*, Vol. 15, No.4, pp. *818-827* (2006)

[23] D. M. Phillips: "Determination of gas temperature from unresolved bands in the spectrum from a nitrogen discharge", *J. Phys. D: Appl. Phys.,* Vol. 9, No.3, pp. 507-521 (1976)

[24] C.O. Laux, T.G. Spence, C.H. Kruger and R.N. Zare: "Optical diagnostics of atmospheric pressure air plasmas",*Plasma Sources Sci.Technol.*, Vol.12,No., pp.125-138(2003)

[25] J.M. Luque, M.D. Calzada and M. S´aez: "Experimental research into the influence of ion dynamics when measuring the electron density from the Stark broadening of the Hα and Hβ lines", *J. Phys. B: At. Mol. Opt. Phys.*, Vol.36, No.8, pp.1573-1584 (2003)

[26] M. Y. Qian, C. S. Ren, D. Z. Wang, J. L. Zhang and G. D. Wei: "Stark broadening measurement of the electron density in an atmospheric pressure argon plasma jet with double-power electrodes", *J.Appl. Phys.*, Vol.107, No. 6, pp.063303 (2010)